Journal of Materials Processing Technology, Volume 255, May 2018, pp. 347-353
DOI: 10.1016/j.jmatprotec.2017.12.019

Microstructure and mechanical properties of double-wire + arc additively manufactured Al-Cu-Mg alloys

Zewu Qi [a, b], Baoqiang Cong [a, b, *], Bojin Qi [a, b], Hongye Sun [a, b], Gang Zhao [a, b], Jialuo Ding [c]

[a] *School of Mechanical Engineering and Automation, Beihang University, Beijing, P.R. China 100191*

[b] *MIIT Key Laboratory of Aeronautics Intelligent Manufacturing, Beijing, P.R. China 100191*

[c] *Welding Engineering and Laser Processing Centre, Cranfield University, Cranfield, MK430AL, UK*

Abstract As the properties of wire + arc additively manufactured Al-6.3Cu alloy cannot meet the applying requirements, a double-wire + arc additive manufacturing system was built to add magnesium into Al-Cu deposits for higher mechanical properties. Two commercial binary wires aluminum-copper ER2319 and aluminum-magnesium ER5087 were chosen as the filler metal to build Al-Cu-Mg components with different compositions by adjusting the wire feed speed. The microstructure and morphology of thin wall samples were characterized by optical micrographs (OM), X-ray diffraction (XRD) and scanning electron microscopy (SEM). The Vickers hardness and tensile properties were investigated. The microstructure of Al-Cu-Mg deposits was mainly composed of coarse columnar grains and fine equiaxed grains with non-uniformly distributing characteristics. With higher Cu but lower Mg content, the strengthen phase turned to Al_2Cu + Al_2CuMg from Al_2CuMg, and the micro hardness presented an increasing trend. The isotropic characteristics of ultimate tensile strength (UTS), yield strength (YS) and elongation were revealed in these samples. The UTS was about 280±5 MPa both in horizontal and vertical directions for all samples. The YS showed an increasing trend from 156MPa to 187MPa with the same content trend, while elongation decreased from 8.2% to 6%. The fractographs exhibited typical brittle fracture characteristics.

---

* Corresponding author.

E-mail address: congbq@buaa.edu.cn (B. Cong).

Published by Elsevier. This is the Author Accepted Manuscript issued with: Creative Commons Attribution Non-Commercial No Derivatives License (CC:BY:NC:ND 4.0).
The final published version (version of record) is available online at DOI:10.1016/j.jmatprotec.2017.12.019. Please refer to any applicable publisher terms of use.

Keywords: double-wire + arc additive manufacturing; Al-Cu-Mg alloy; microstructure; mechanical properties

1 Introduction

Additive manufacturing (AM) technique is a new technology for directly fabricating components through depositing material layer-by-layer. In comparison to conventional machining processes for producing metallic structures, AM has drawn significant attentions due to its potential benefits of saving lead time and cost (Williams et al., 2016). Classified according to the employed heat source, such as laser, electron beam and arc, or the used feedstock, such as powder and wire, a variety of AM processes can be used to fabricate metallic structures (Oguzhan and Adnan, 2016). The arc and wire based AM process is often referred to as wire + arc additive manufacturing (WAAM), in which the filling wire is melted by the heat of arc and deposited along the designed route in a layer-by-layer fashion. WAAM shows its advantages on manufacturing large-scale metallic components for its high deposition rate and material utilization rate with comparatively low production and equipment cost among different AM processes (Martina et al., 2012). High strength aluminum alloys have been extensively used in aerospace and military applications due to their excellent mechanical properties (Starke and Staley, 1996). Applying WAAM technology to produce high strength aluminum alloy shows an interest and requirement from aerospace industries.

For aluminum alloys WAAM technology, the employed heat sources, wires, process parameters and further treatments are the research focuses to control the formation, microstructure and mechanical properties of the components. Ding et al. (2014a) presented an algorithm to automatically generate optimal tool-paths for WAAM process with a large class of geometries, and the proposed path planning strategy shows better surface accuracy in comparison with the existing hybrid methods. Ding et al. (2014b) provided a transient thermomechanical finite element model to investigate the stress evolution during the thermal cycles of WAAM process and predict the distortion and residual stress. Geng et al. (2017) developed a mathematical model for calculating the wire flying distance in arc zone, in order to ensure the size accuracy of the components with gas tungsten arc welding (GTAW) WAAM process. Gu et al. (2014) reported the internal and external properties of the filling wires has great influence on the performance of the WAAM

parts. Gu et al. (2016a) also pointed out that the inter-layer cold working and post-deposition heat treatment can efficiently eliminate the porosity defects in WAAM 2319 aluminum alloy. Cong et al. (2015) systemically studied the effect of arc mode in cold metal transfer (CMT) process on the porosity characteristic of WAAM Al-6.3%Cu alloy, and found the CMT pulse advanced mode is the most suitable process for depositing aluminum alloy due to its excellent performance in controlling porosity. Cong et al. (2017) further found the porosity, microstructure and micro hardness varied with the CMT variants and depositing paths.

Among different kinds of high strength aluminum alloys, Al-Cu alloy of 2000 series is particularly in a favor because of its wide aerospace applications such as cryogenic tanks, fuselage or shells for space vehicles, as described by Naga et al. (2007). The ultimate tensile strength (UTS) of wrought 2219-T8 alloy is up to 455 MPa, however, it cannot reach this level with WAAM process. As illustrated by Bai et al. (2016), the UTS of as-deposited WAAM 2219-Al alloy is only 237 MPa with variable polarity GTAW (VP-GTAW) process, and 250 MPa using pulse advanced CMT as the heat source (Gu et al. 2016b). The mechanical properties of as-deposited WAAM aluminum alloys need to be enhanced to meet the applying requirement. Bai et al. (2017) adopted solution + aging technique to treat GTA-additively manufactured 2219-Al alloy, and found the UTS can be improved to 391 ± 28 MPa after heat treatment. Gu et al. (2016b) introduced inter-layer rolling technique to WAAM Al-6.3Cu alloy, and found the UTS can be enhanced significantly, which is up to 450MPa. Adding chemical elements into Al-Cu alloy is also an idea for achieving higher mechanical properties. For example, AA2024 is a representative Al-Cu-Mg alloy, which has been widely used in missile or airscrew for space vehicles. The mechanical properties of Al-Cu-Mg alloys vary with different copper and magnesium content. An idea of manufacturing Al-Cu-Mg alloys was lighten to obtain higher mechanical properties. However, there is no such a variety of standard Al-Cu-Mg wires with different copper and magnesium content for building WAAM Al-Cu-Mg alloys.

In this paper a double-wire + arc additive manufacturing system was built, ER2319 (Al-6.3 wt% Cu) wire and ER5087 (Al-5 wt% Mg) wire were used for building Al-Cu-Mg components with different compositions (Al-3.6Cu-2.2Mg, Al-4Cu-1.8Mg and Al-4.4Cu-1.5Mg) by adjusting the wire feed speed. The

microstructure and mechanical properties of these WAAM Al-Cu-Mg alloys were investigated.

2 Experimental

Experiments were carried out with double-wire + arc additive manufacturing (D-WAAM) system, which mainly consisted of a VP-GTAW power supply, a GTAW torch, a shielding gas system, a working table, a water-cooling system, a moving control system, two wire feeders and a double-wire device, as shown in Fig.1. Two commercial binary wires aluminum-copper ER2319 and aluminum-magnesium ER5087 were chosen as the filler metal, and 2A12 as the substrate. The nominal compositions of ER2319 and ER5087 wires (both 1.2 mm in diameter) and 2A12 substrates (320 mm × 150 mm × 12 mm in dimension) are listed in Table 1. The substrates were washed in alkaline water and dried in air, and then cleaned with mechanical method and degreased using acetone before deposition.

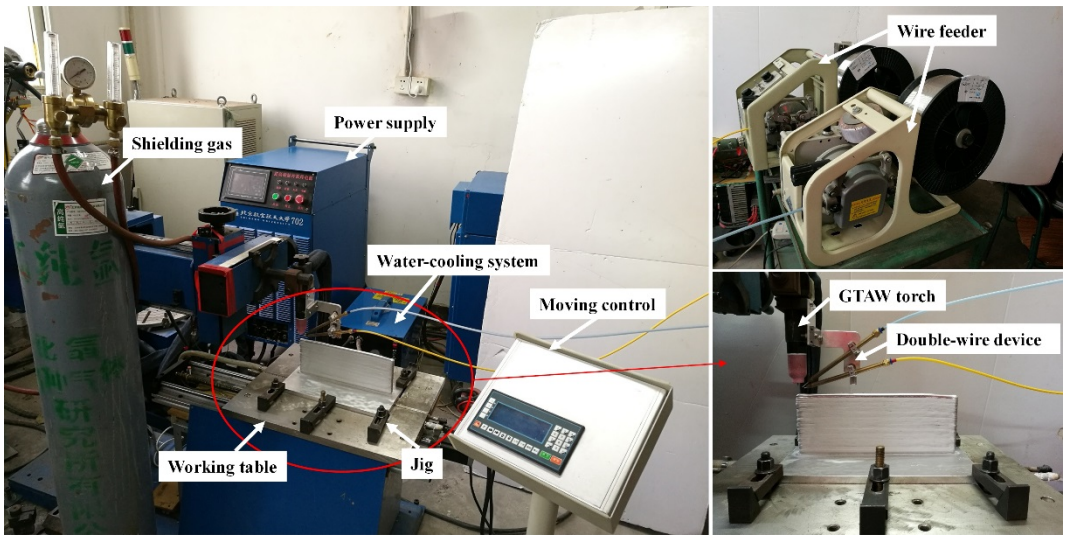

Fig.1. Double-wire + arc additive manufacturing system

Table 1

Nominal composition of ER2319, ER5087 wire and 2A12 substrate

Alloys	ρ	Composition （wt.%）							
	g/cm^3	Cu	Mg	Si	Mn	Zr	Fe	Ti	Al
ER2319	2.77	6.3	-	0.04	0.28	0.19	0.1	0.145	Bal.
ER5087	2.66	-	5.05	0.05	0.74	0.12	0.1	0.114	Bal.
2A12	2.75	4.3	1.5	0.5	0.6	-	0.5	0.20	Bal.

Different from single wire + arc additive manufacturing process, two wires were fed in front of the arc through two wire feeders and the double-wire device, melting and flowing into the molten pool in double-wire + arc additive manufacturing process, as shown in Fig.2. The amount of copper and magnesium content can be regulated by adjusting the wire feed speed (*WFS*). The mass fraction (*E*) of main elements can be calculated using

$$E=\frac{\sum WFS_i D_i^2 \rho_i E_x}{\sum WFS_i D_i^2 \rho_i}$$

where E_x (x=Cu, Mg) is the mass fraction of element in a certain wire, WFS_i (i=1, 2) is the wire feed speed, D_i (i=1, 2) is the diameter of the wire, ρ_i (i=1, 2) is the density of the wire. Thin wall samples (280mm×105mm×7mm in dimension) were manufactured with three compositions (Al-3.6Cu-2.2Mg, Al-4Cu-1.8Mg and Al-4.4Cu-1.5Mg). The VP-GTAW arc current (120A, 100Hz and DCEN:DCEP = 4:1), travel speed (300mm/min), Ce-W electrode (3.2 mm in diameter and 60° in vertex angle), cathode tip to work distance (5 mm) and shielding gas flow rate (18 L/min) of normal pure argon (99.99%) were kept constant for all the samples. Other parameters of D-WAAM components are shown in Table 2.

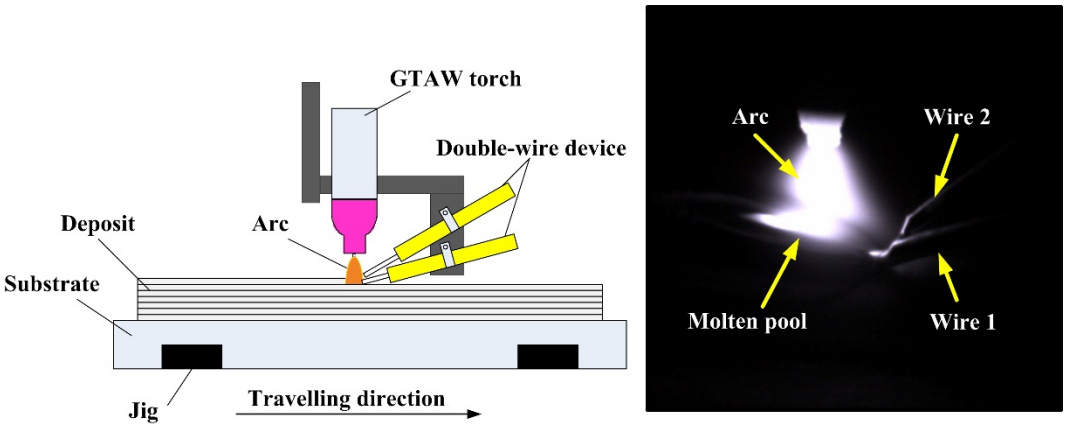

Fig.2. Depositing model of D-WAAM process

Table 2

Parameters of the D-WAAM aluminum alloys

Compositions	Wire feed speed(m/min)		E(wt.%)		E_{Cu}/E_{Mg}
	ER2319	ER5087	Cu	Mg	
Al-3.6Cu-2.2Mg	1.50	1.20	3.57	2.19	1.6
Al-4.0Cu-1.8Mg	1.80	1.05	4.04	1.81	2.2
Al-4.4Cu-1.5Mg	2.40	1.05	4.44	1.49	3.0

Samples for testing were sectioned as shown in Fig.3a. Both ends (15 mm) of each wall were cut off and discarded. Samples for microstructure and micro hardness tests were taken from the middle part of the wall. Three tensile test samples along vertical direction were equidistantly taken from middle to the end of the wall. Another three tensile test samples in horizontal direction were evenly taken from the top to the root of each wall. The tensile test samples were machined in standard, as shown in Fig.3b. Tensile tests were carried out at ambient temperature by an electro-mechanical universal testing machine (SANS 5504) with 1.5 mm/min loading rate. Vickers micro hardness testing machine (FM800) was employed to measure the micro hardness with 1.96 N load for 15 s. Hardness test started 50 mm from the bottom of each wall. Thirty micro hardness tests with an interval of 0.5 mm were taken along the vertical direction.

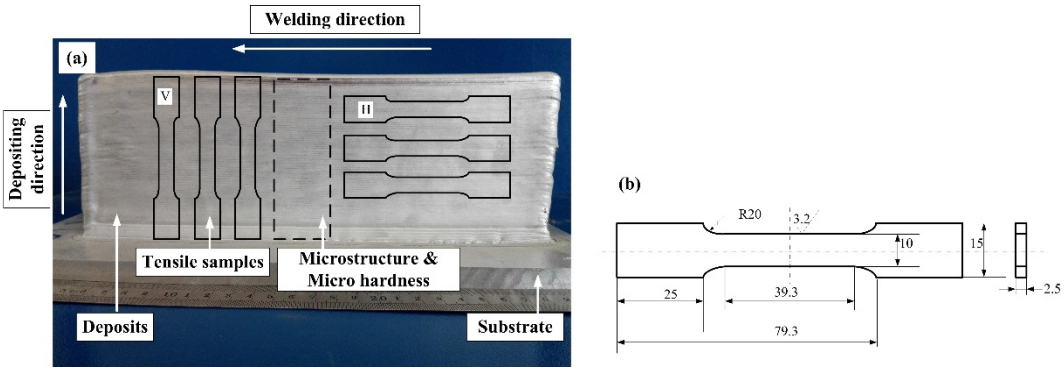

Fig.3. (a) The sampling positions of each wall; (b) the size of tensile sample

Optical microscopy (OM) (LEICA DM4000) was employed to observe the microstructure. X-ray diffraction (XRD) tests were conducted with X-ray diffractometer (D/Max-2200pc) for phase analysis. Energy dispersive spectrometry (EDS) detected with scanning electron microscopy (SEM) (Camscan-3400) was used for micro-area composition analysis. The specimens were ground with 400, 800, 1200, 1500, 2000 and 2500 waterproof abrasive paper, and then polished with 3μm diamond paste and SiO_2 suspension. XRD and SEM tests were conducted firstly. Etching was performed with Keller's reagent solution before OM tests. Fracture surface morphology of the tensile specimens was performed using SEM.

3 Results and discussion

3.1 Microstructure

Obvious layer characteristics of the microstructure in WAAM Al-Cu-Mg alloys with different compositions can be seen in Fig.4. Each deposited layer is

divided into inner-layer region and inter-layer region (Fig.4a, Fig.4d and Fig.4g). The microstructure in different regions shows different morphology. In inner-layer region, the microstructure is mainly composed of coarse columnar grains and fine equiaxed grains with non-uniformly distributing characteristics. As shown in Fig.4b and Fig.4e, most grains present non-dendritic characteristic with only a small amount of dendritic grains in inner-layer region of Al-3.6Cu-2.2Mg and Al-4Cu-1.8Mg alloys, while equiaxed dendritic grains and columnar dendritic grains become the dominant grains in inner-layer region of Al-4.4Cu-1.5Mg (Fig.4h). The microstructure in inter-layer region reveals equiaxed non-dendritic characteristic in Al-3.6Cu-2.2Mg (Fig.4c) and Al-4Cu-1.8Mg alloys (Fig.4f), and equiaxed dendritic characteristic in Al-4.4Cu-1.5Mg alloys (Fig.4i).

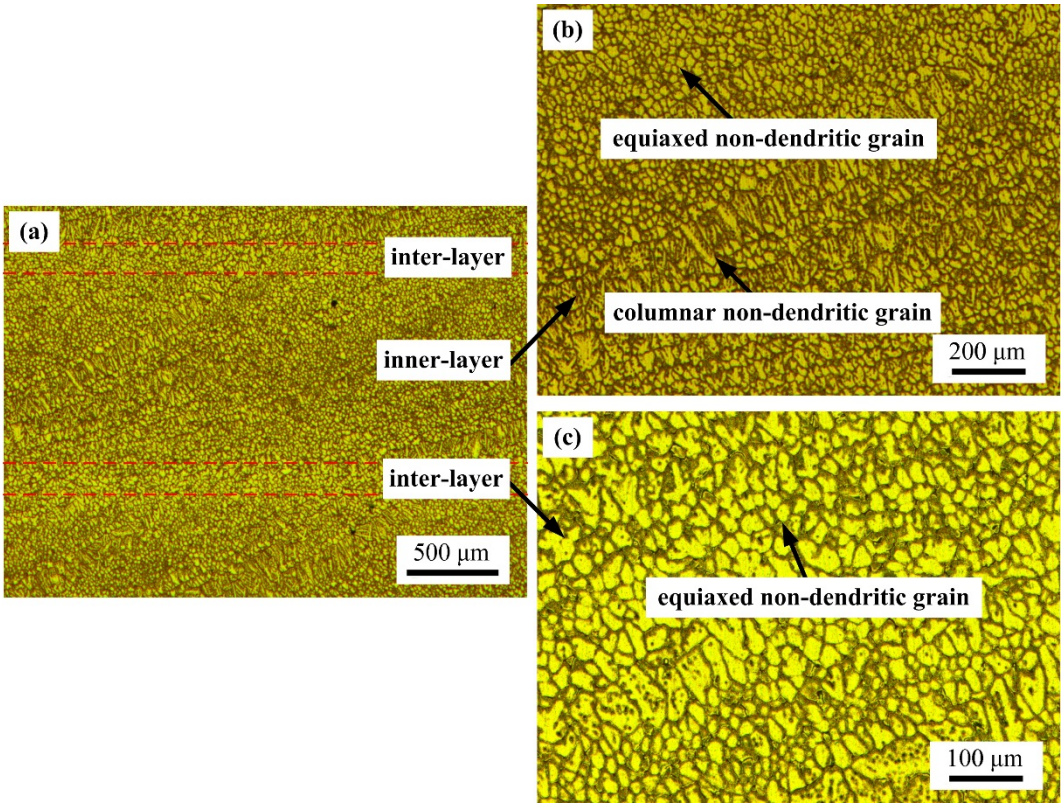

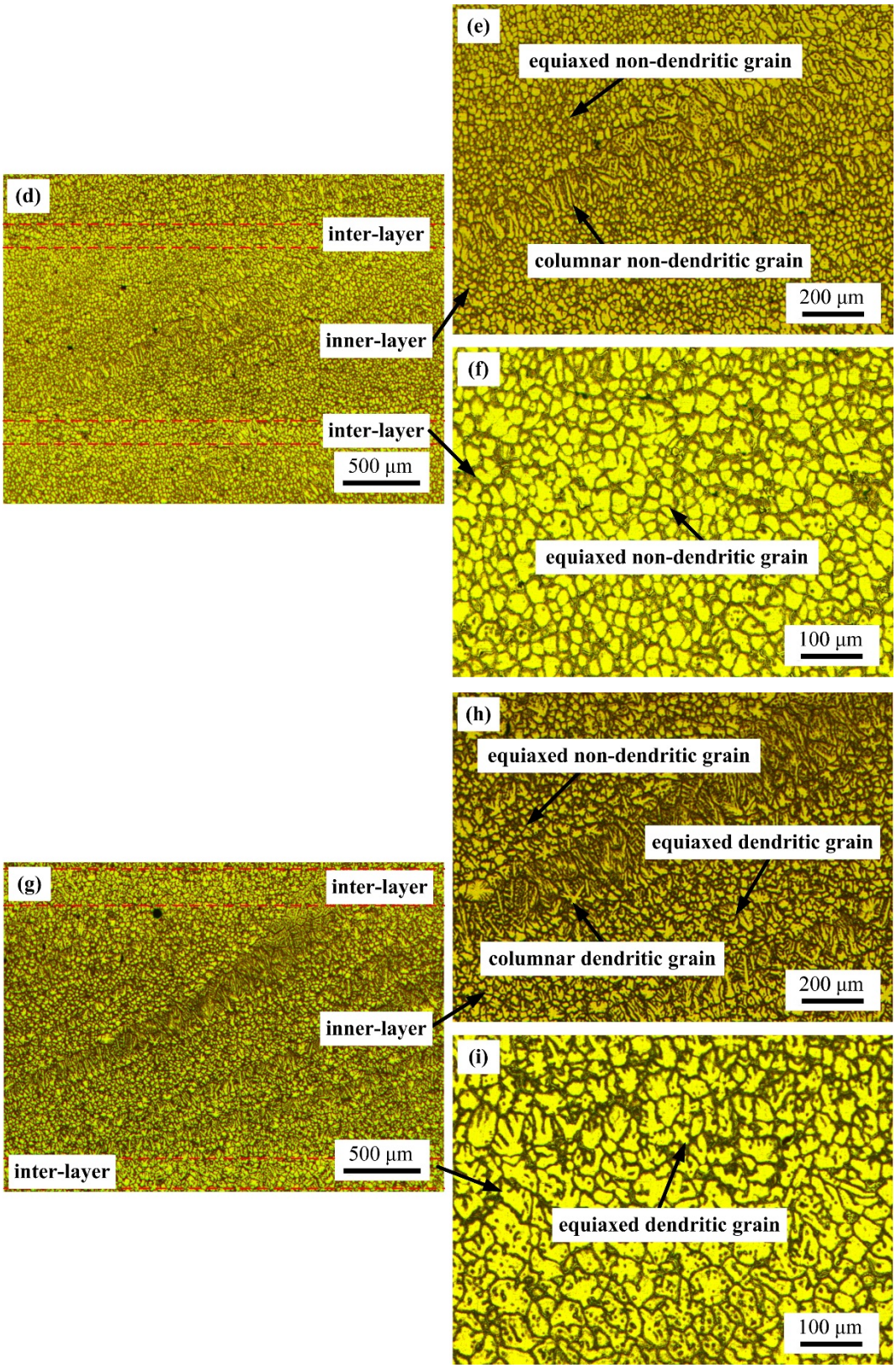

Fig.4. Optical micrographs for the WAAM Al-Cu-Mg alloys: (a) Al-3.6Cu-2.2Mg, (b) inner-layer of Al-3.6Cu-2.2Mg, (c) inter-layer of Al-3.6Cu-2.2Mg, (d) Al-4Cu-1.8Mg, (e) inner-layer of Al-4Cu-1.8Mg, (f) inter-layer of Al-4Cu-1.8Mg, (g) Al-4.4Cu-1.5Mg, (h) inner-layer of Al-4.4Cu-1.5Mg, (i) inter-layer of Al-4.4Cu-1.5Mg

Fig.5 presents the XRD patterns of these WAAM Al-Cu-Mg alloys. It can be found that the phases are mainly α-Al and S phase (Al_2CuMg) in Al-3.6Cu-2.2Mg alloy; α-Al, S phase and θ phase (Al_2Cu) in Al-4Cu-1.8Mg and Al-4.4Cu-1.5Mg alloy from the XRD results as shown in Fig.5. With higher Cu but lower Mg content, there is an increasing trend of θ phase. The results are in accordance with the solidification pathways for Al-Cu-Mg alloys using Scheil analysis, as shown in Fig.6 (Pickin et al., 2009). Compositions which start as α-Al and terminate in an isothermal eutectic reaction ($\alpha + \theta + S$) are presented with the first solid line. Each side of this line, red, green and pink regions are compositions which start as α-Al but terminate in non-isothermal eutectic reactions ($\alpha + \theta + S$, $\alpha + \theta + S$ and $\alpha + \gamma + S$, respectively). There is another solid line separating the green and pink regions, where quasi-binary eutectic reaction ($\alpha + S$) occurs during the solidification of components with the same chemical compositions. The deposited Al-3.6Cu-2.2Mg alloy is sited in the second solid line with α-Al and S phase in the components, while Al-4Cu-1.8Mg and Al-4.4Cu-1.5Mg alloys are respectively located in green and red zone with α-Al, S phase and θ phase inside.

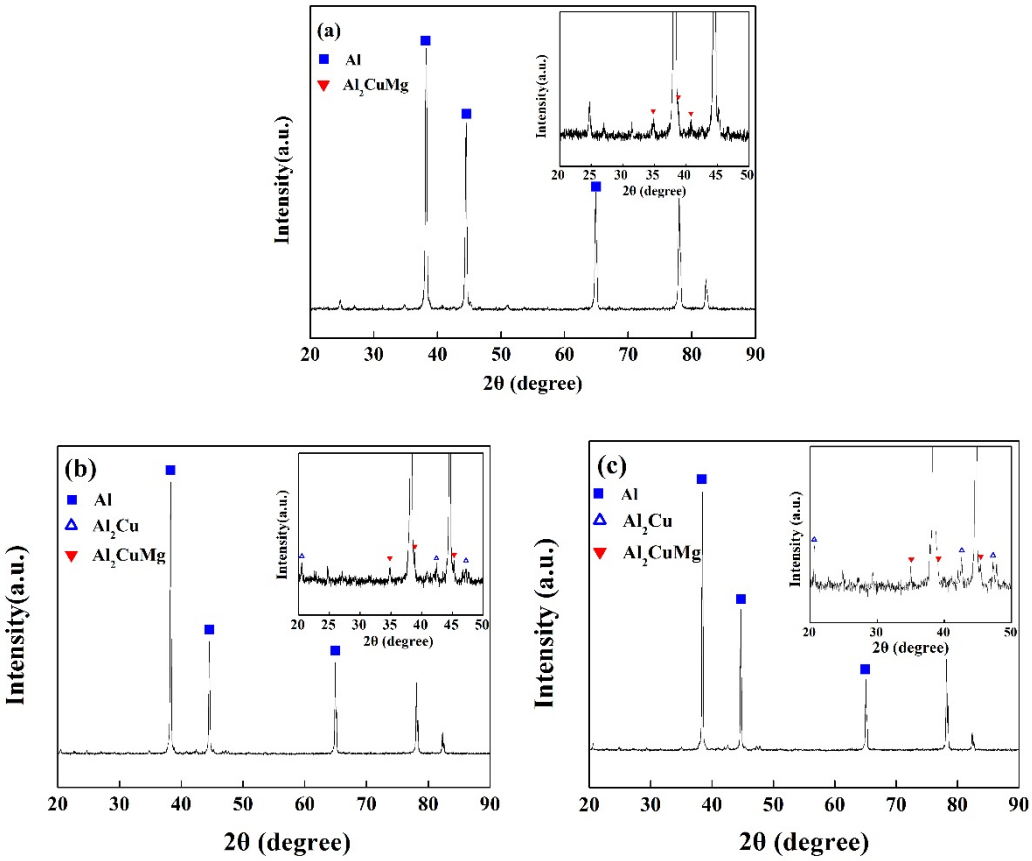

Fig.5. The XRD results of WAAM Al-Cu-Mg alloys. (a) Al-3.6Cu-2.2Mg; (b) Al-4Cu-1.8Mg; (c) Al-4.4Cu-1.5Mg

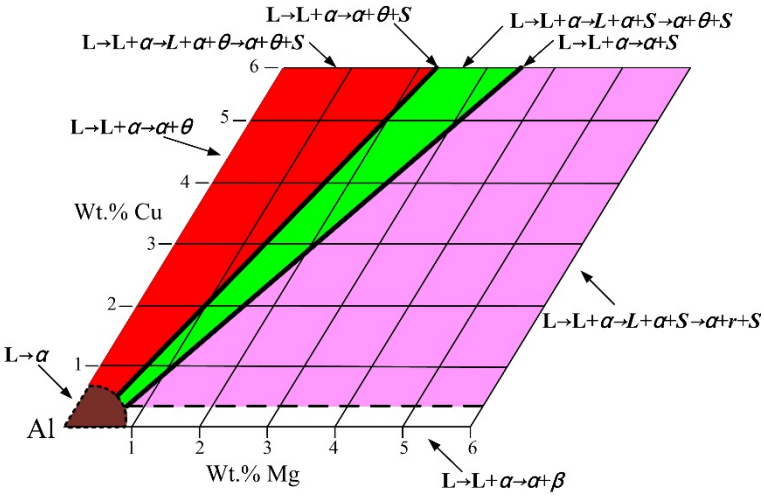

Fig.6. Solidification pathways for Al-Cu-Mg alloys

The SEM images with EDS results are exhibited in Fig.7. The white second phase particles net-likely distribute along the grain boundaries or scatter in the grain. Analyzed using EDS, the second phase particle with bright white color is *θ* phase, and with dark white color is *S* phase. With higher Cu but lower Mg content, the content of second phase particles with bright white color (θ phase) gradually increase, as shown from Fig.7a to Fig.7c. This phenomenon is consistent with the XRD results. The *S* phases mainly net-likely distribute along the grain boundary in aluminum matrix. As Cu content increased and Mg content decrease, *θ* phases generate and punctiformly scatter in the cross section of the grain boundary or in the interior of the grains.

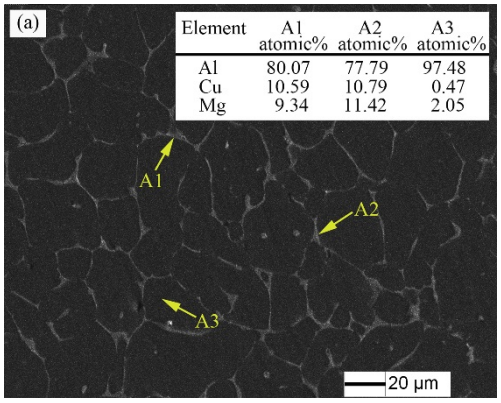

Element	A1 atomic%	A2 atomic%	A3 atomic%
Al	80.07	77.79	97.48
Cu	10.59	10.79	0.47
Mg	9.34	11.42	2.05

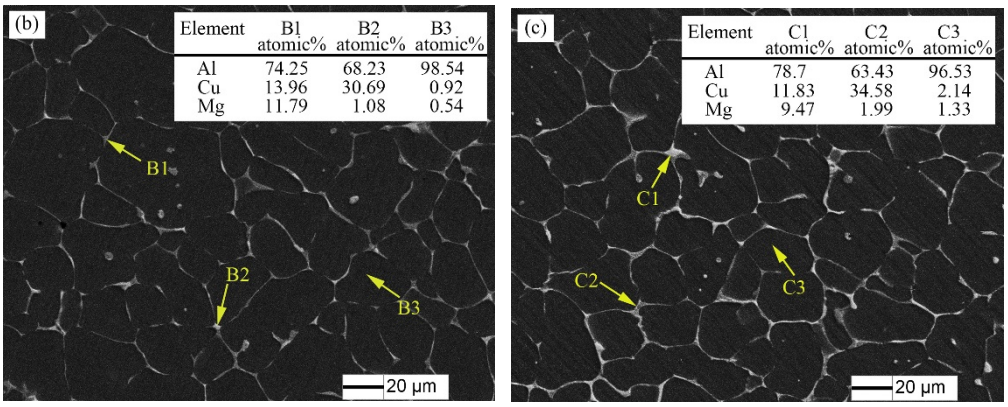

Fig.7. Scanning electron micrographs and energy dispersive spectrometry results of WAAM Al-Cu-Mg alloys. (a) Al-3.6Cu-2.2Mg; (b) Al-4Cu-1.8Mg; (c) Al-4.4Cu-1.5Mg

3.2 Micro hardness

The micro hardness test results of the deposited alloys are shown in Fig.8. Hardness value varying with the content of copper and magnesium can be observed. There is an increasing trend between the micro hardness and Cu/Mg ratio. The average hardness value are 86 HV, 90 HV and 95 HV respectively in Al-3.6Cu-2.2Mg, Al-4Cu-1.8Mg and Al-4.4Cu-1.5Mg alloys. In comparison to the hardness value (77.5 HV) of WAAM 2219-Al (Al-6.3%Cu) deposits (Bai et al. 2016), the hardness can be improved by adding Mg element. The difference of micro hardness value along vertical direction increase with higher Cu/Mg ratio (Fig.9), indicating mechanical properties of Al-Cu-Mg WAAM deposits are gradually uneven with increased Cu/Mg ratio.

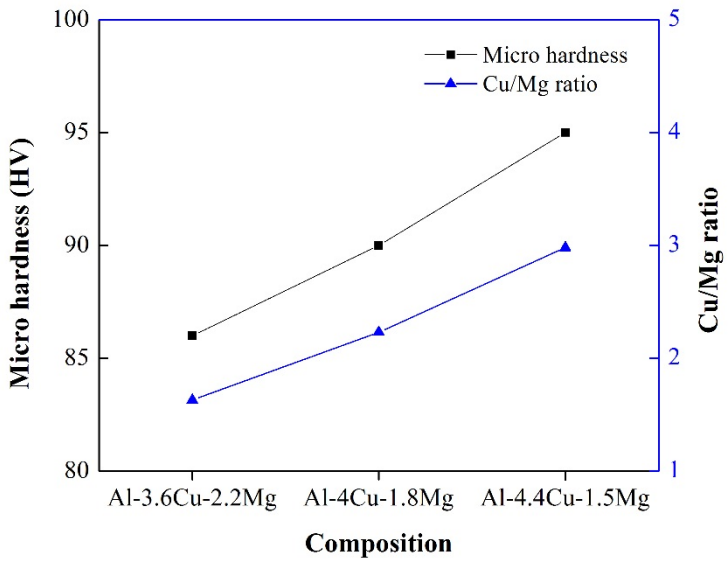

Fig.8. Micro hardness of WAAM Al-Cu-Mg alloys with different compositions

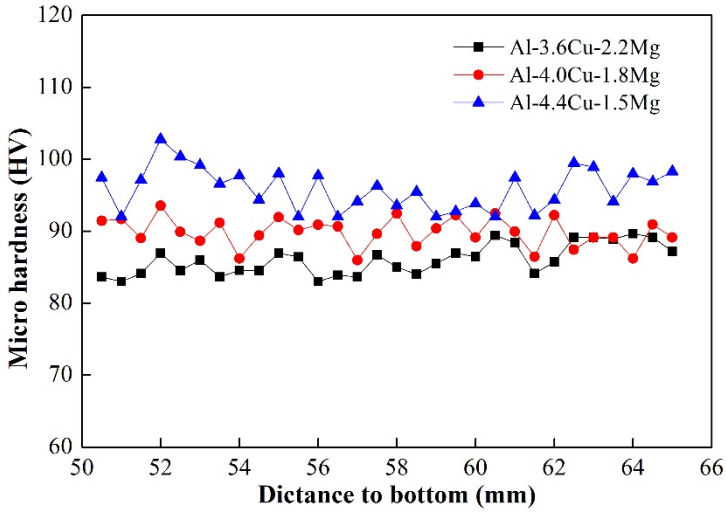

Fig.9. Micro hardness distribution of WAAM Al-Cu-Mg alloys

3.3 Tensile properties

Fig.10 reveals the ultimate tensile strength (UTS), yield strength (YS) and elongation results of these components. The strength properties show an isotropic characteristic, with only 3 - 7MPa difference of UTS, 2 - 5MPa difference of YS and 0.1% - 0.4% difference of elongation between the mechanical properties in horizontal and vertical directions. The properties in horizontal direction are superior to the one in vertical direction. The UTS of these WAAM Al-Cu-Mg alloys is around 280 ± 5MPa. The YS presents an increasing trend from 156 MPa to 177 MPa in horizontal direction with higher Cu but lower Mg content, however, there is a decreasing trend from 8.2% to 6% of the horizontal elongation with the same element content trend. Compared to the mechanical properties of WAAM 2219-Al (Al-6.3%Cu) component (UTS: 237 MPa, YS: 112 MPa, Elongation: 10.7%) (Bai et al. 2016), the strength properties are improved by adding right amount of magnesium, but the plasticity is reduced .

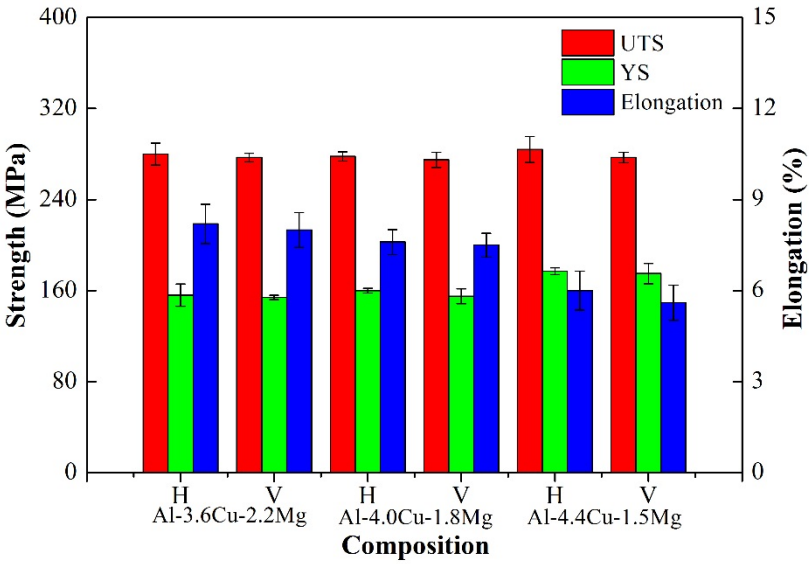

Fig.10. Tensile properties of WAAM Al-Cu-Mg alloys

The appearance of fracture surfaces investigated by SEM for these WAAM Al-Cu-Mg alloys both in horizontal and vertical directions are shown in Fig.11. The same fracture characteristics are presented in all the samples with different compositions. The fractographs exhibit typical brittle fracture characteristics. It can be found that the dominant fracture mode is intergranular fracture, which is regarded as an indication of brittle fracture. There is also some dimples on the fracture surface, however, the number of dimples is few. It cannot be regarded as ductile fracture characteristics. Some second cracks are distributed in the fractured surface as well. When a static load is applied to the deposits, these second cracks can grow and become the fracture source.

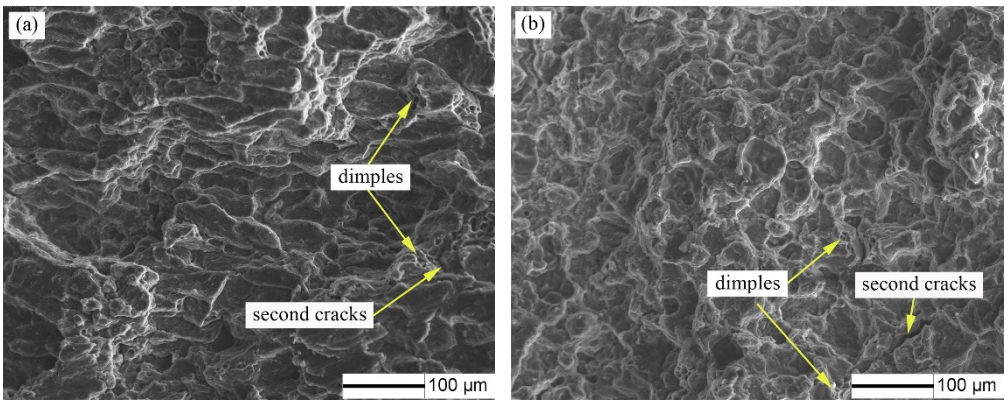

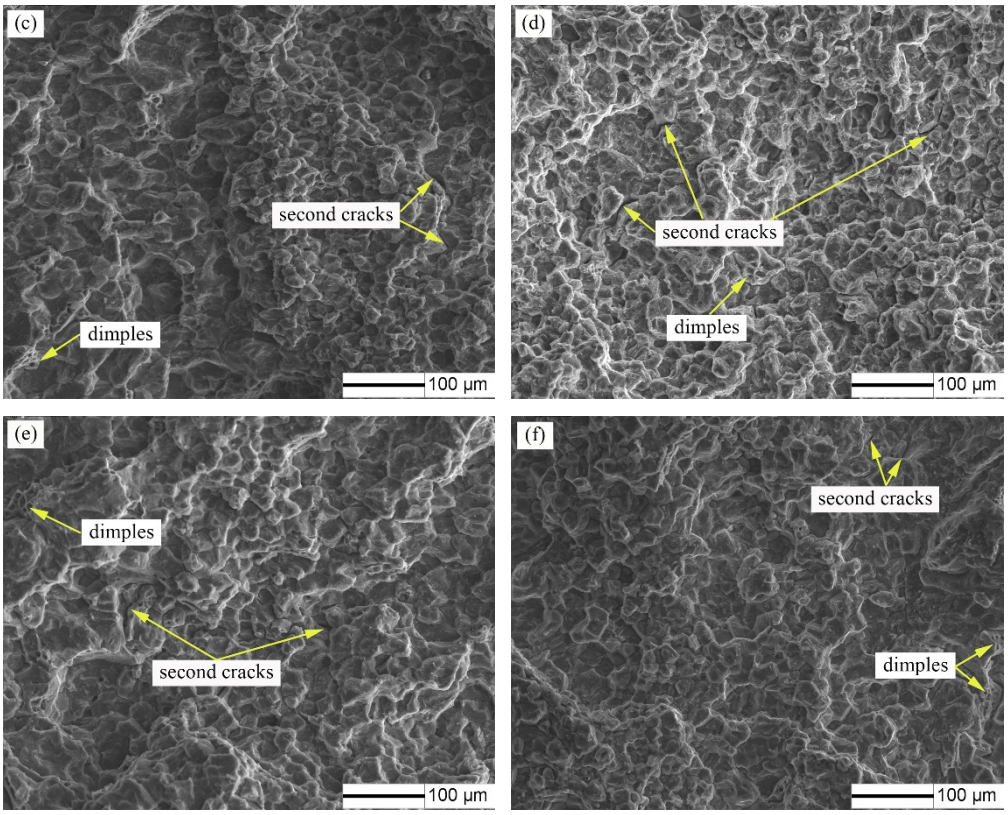

Fig.11. SEM images of fracture surface for: (a) Al-3.6Cu-2.2Mg, (c) Al-4Cu-1.8Mg and (e) Al-4.4Cu-1.5Mg in horizontal direction; (b) Al-3.6Cu-2.2Mg, (d) Al-4Cu-1.8Mg and (f) Al-4.4Cu-1.5Mg in vertical direction

4 Conclusions

In this study, ternary Al-Cu-Mg deposits with different compositions (Al-3.6Cu-2.2Mg, Al-4Cu-1.8Mg and Al-4.4Cu-1.5Mg) were achieved by D-WAAM process through adjusting the wire feed speed of ER2319 and ER5087. The microstructure and mechanical properties of these Al-Cu-Mg samples were investigated systematically. The conclusions can be drawn as following:

(1) The microstructure of Al-Cu-Mg deposits mainly consisted of coarse columnar grains and fine equiaxed grains with non-uniformly distributing characteristics in inner-layer region, and equiaxed grains in inter-layer region.

(2) The phases in Al-3.2Cu-2.2Mg were mainly α-Al and S phase. With higher Cu but lower Mg content, θ phase gradually generated and increased.

(3) The micro hardness ranged from 86 HV to 95 HV with increased Cu/Mg ratio. Compared with the hardness of Al-6.3%Cu deposits (77.5 HV), the micro hardness can be improved.

(4) The UTS was around 280MPa. The YS showed an increasing trend from 156 MPa to 187 MPa along with higher Cu/Mg ratio. The strength properties can be

significantly enhanced by adding right amount of magnesium.

(5) Typical brittle fracture characteristics were exhibited in the fracture surfaces.

Acknowledgements

The authors are grateful to be supported by Beijing Municipal Science and Technology Commission and the Fundamental Research Funds for the Central Universities (Grant No.YWF-16-GJSYS-19), and the WAAMMat Programme (www.waammat.com).

References

Bai, J., Yang, C., Lin, S., Dong, B., Fan, C., 2016. Mechanical properties of 2219-Al components produced by additive manufacturing with TIG. International Journal of Advanced Manufacturing Technology 86, 479-485.

Bai, J., Fan, C., Lin, S., Yang, C., Dong, B., 2017. Mechanical properties and fracture behaviors of GTA-additive manufactured 2219-Al after an especial heat treatment. Journal of Materials Engineering and Performance 26, 1808-1816.

Cong, B., Ding, J., Williams, S.W., 2015. Effect of arc mode in cold metal transfer process on porosity of additively manufactured Al-6.3% Cu alloy. International Journal of Advanced Manufacturing Technology 76, 1593–1606.

Cong, B., Qi, Z., Qi, B., Sun, H., Zhao, G., Ding, J., 2017. A comparative study of additively manufactured thin wall and block structure with Al-6.3%Cu alloy using cold metal transfer process. Applied Sciences Basel 7, 275.

Ding, D., Pan, Z., Cuiuri, D., Li, H., 2014a. A tool-path generation strategy for wire and arc additive manufacturing. International Journal of Advanced Manufacturing Technology 73, 173-183.

Ding, J., Colegrove, P., Mehnen J., Williams S.W., Wang, F., Sequeira A.P., 2014b. A computationally efficient finite element model of wire and arc additive manufacture. International Journal of Advanced Manufacturing Technology 70, 227-236.

Geng, H., Li, J., Xiong, J., Lin, X., Zhang, F., 2017. Optimization of wire feed for GTAW based additive manufacturing. Journal of Materials Processing Technology 243, 40-47.

Gu, J., Ding, J., Cong, B., Bai, J., Gu, H., Williams, S.W., Zhai, Y., 2014. The influence of wire properties on the quality and performance of Wire + Arc Additive Manufactured aluminum parts. Advanced Materials Research 1081, 210–214.

Gu, J., Ding, J., Williams, S.W., Gu, H., Ma, P., Zhai, Y., 2016a. The effect of inter-layer cold working and post-deposition heattreatment on porosity in additively manufactured aluminum alloys. Journal of Materials Processing Technology 230, 26-34.

Gu, J., Ding, J., Williams, S.W., Gu, H., Bai, J., Zhai, Y., Ma, P., 2016b. The strengthening effect of inter layer cold working and post-deposition heat treatment on the additively manufactured Al–6.3Cu alloy. Materials Science and Engineering A 651, 18–26.

Martina, F., Mehnen J., Williams S.W., Colegrove, P., Wang F., 2012. Investigation of the benefits of plasma deposition for the additive layer manufacture of Ti-6Al-4V. Journal of Materials Processing Technology 212, 1377-1386.

Naga Raju, P., Srinivasa Rao, K., Reddy, G.M., Kamaraj, M., Prasad Rao, K, 2007. Microstructure and high temperature stability of age hardenable AA2219 aluminum alloy modified by Sc, Mg and Zr additions 464, 192–201.

Oguzhan Y., Adnan A.U., 2016. Shaped metal deposition technique in additive manufacturing technology: a review. Proceedings of the Institution of Mechanical Engineers, Part B: Journal of Engineering Manufacture 230, 1781-1798.

Pickin, C.G., Williams, S.W., Prangnell, P.B., Robson, J., Lunt, M., 2009. Control of weld composition when welding high strength aluminum alloy using the tandem process. Science and Technology of Welding and Joining 14, 734-739.

Starke Jr., E.A., Staley, J.T. 1996. Application of modern aluminum alloys to aircraft. Progress in Aerospace Sciences 32, 131–172.

Williams, S.W., Martina, F., Addison, A.C., Ding, J., Pardal, G., Colegrove, P., 2016. Wire plus Arc Additive Manufacturing. Journal of Materials Science and Technology 32, 641–647.

Cranfield University

CERES https://dspace.lib.cranfield.ac.uk

School of Aerospace, Transport and Manufacturing (SATM) Staff publications (SATM)

2017-12-16

Microstructure and mechanical þÿproperties of double-wire/+/ar additively manufactured Al-Cu-Mg alloys

Qi, Zewu

Elsevier

Qi Z, Cong B, Qi B, et al., (2018) Microstructure and mechanical properties of
þÿdouble-wire/+/arc additively manufactured Al-Cu-Mg alloys. Journal of M
Technology, Volume 255, May 2018, pp. 347-353
https://doi.org/10.1016/j.jmatprotec.2017.12.019
Downloaded from Cranfield Library Services E-Repository